Backscatter Transponder Based on Frequency Selective Surface for FMCW Radar Applications

Antonio LAZARO, Javier LORENZO, Ramon VILLARINO, David GIRBAU

Dept. of Electronics, Electrics and Automatic Control Engineering, Rovira i Virgili University,
Av.Països Catalans 26, 43007 Tarragona, Spain

antonioramon.lazaro@urv.cat, javier.lorenzo@urv.cat, ramonvillarino@urv.cat, david.girbau@urv.cat

Abstract. *This paper describes an actively-controlled frequency selective surface (FSS) to implement a backscatter transponder. The FSS is composed by dipoles loaded with switching PIN diodes. The transponder exploits the change in the radar cross section (RCS) of the FSS with the bias of the diodes to modulate the backscattered response of the tag to the FMCW radar. The basic operation theory of the system is explained here. An experimental setup based on a commercial X-band FMCW radar working as a reader is proposed to measure the transponders. The transponder response can be distinguished from the interference of non-modulated clutter, modulating the transponder's RCS. Some FSS with different number of dipoles are studied, as a proof of concept. Experimental results at several distances are provided.*

Keywords

Transponder, FMCW radar, Frequency Selective Surface (FSS), RFID.

1. Introduction

FMCW (Frequency Modulated Continuous Wave) radar differs from pulsed radar in that an electromagnetic signal is continuously transmitted [1]. The FMCW radar emits a RF signal that is usually swept linearly in frequency. The received signal is then mixed with the emitted signal and due to the delay caused by the time of flight for the reflected signal, a frequency difference, called beat frequency, is produced. The range from the radar to the target is proportional to the beat frequency. Due to their ability to determine range, FMCW based systems are commonly used for measuring distances in applications such as tank level gauging, where high resolution non-contact measurements in harsh conditions are required [2]. Other common applications include automotive collision avoidance radars [3], [4], altimetry [1], or marine radars [5]. It is also proposed for wall-penetrating radar with the object of imaging and detection applications, security sensors against intrusion [6], and human vital-sign detection and measurement [7]. In recent years, FMCW radar has been proposed in the literature for wireless local positioning systems [8]-[10]. It has also been used as reader for long distance transponders, integrating different types of sensors such as pressure [11], [12] or temperature sensors [13].

The major challenges for wireless local positioning systems are disturbances caused by the multipath reflections [14]. Often, parasitic reflections are several orders of magnitude greater than the target. Thus, clutter contamination is an important trouble in several applications such as the determination of the radar cross section of pedestrians, which is lower than that of cars or ground. In other cases, tank walls can produce errors in level gauges [2]. Furthermore, FMCW radars have a minimum measurement distance limited by the antenna coupling and phase noise power that produce a strong interference in the low-frequency part of the output spectrum [1].

In order to mitigate these common problems, a modulated backscatter transponder has been proposed in [14-17]. In this case, the spectrum at the output of the mixer is shifted by the modulated frequency of the transponder or tag, f_{tag} [15]. The range measurement is performed by analyzing the spectrum of the beat signal around f_{tag} and by verifying the presence of a couple of peaks. The frequency difference between peaks is proportional to the distance between the radar and the tag. Several approaches have been employed to implement the backscatter transponder. The simplest is to match/mismatch the output of the antenna's transceiver achieving a modulation of the backscattered field [14], [16]. Retroactive modulated Van Atta arrays [17] have been employed both to reduce multipath effect by using directive antennas and to increase the received signal strength. Another active solution is based on a secondary radar, in which a transponder responds to an interrogating radar signal [18]. Here the main challenge is the delay synchronization between the radar and the transponder [18]. One solution proposed is based on a switched injection locked oscillator transponders [19]. Also, when using a secondary radar, the power consumption of an RF oscillator is notably higher than the power needed to modulate a semi-passive system whose operating principle is based on matching or mismatching the output of the antenna [19]. Therefore, these active solutions are limited by battery life-time. The existing transponders

based on backscattering are limited to a range under 10 m, whereas secondary radars transponders can typically reach a hundred meters at the cost of higher power consumption, more complexity and higher cost.

It is known that the range resolution in a FMCW radar is only limited by the sweep bandwidth [1]. This means that resolution does not depend on the frequency of the RF signal exactly. Thus, the backscatter transponder should support the FMCW radar sweep bandwidth. Sometimes the transponders presented in the literature are narrow band [15], [17], [19].

The frequency selective surfaces (FSS) are periodic structures in each direction of the plane which act as a filter. This filter property has been exploited in several applications [20], [21]. FSS can be frequency tunable, introducing some switching elements (e.g. PIN diode) [22] or tuning elements (e.g. varactors) [23], [24]. Recently, the FSS modulating properties are also proposed in millimeter-wave communications [25], Terahertz Applications [26] and Radio Identification (RFID) tags design [27], [28]. In [27] FSS are used to design narrow-band transponders. However, wide bandwidth of the FSS will be required for the purpose of this work to achieve high resolution. In a recent work [28], the authors show that FSS can be used to modulate the amplitude of time-domain UWB signals. A tunable FSS based on loaded dipoles was used as a variable filter in [28]. In this work, the UWB pulse was filtered and the amplitude of the backscattered UWB pulse was a function of the integrated backscattered field over the entire pulse frequency spectrum. This fact is a fundamental difference between time and frequency-domain backscattered transponders in which the amplitude depends on the differential radar cross section [29] at the interrogating frequency. The aim of this work is to study the feasibility to use FSS as low-power consumption and wide-band backscatter transponders. Here, the large bandwidth that can be achieved with FSS is used to modulate the FMCW interrogating signal. The work demonstrates that the required bandwidth can be achieved using simple FSS based on loaded dipoles with PIN diodes like those used in UWB signals [28]. Depending on the diode state, the frequency response of the FSS is shifted. Therefore, a large differential radar cross section (RCS) can be achieved over a large frequency bandwidth. This frequency bandwidth is often difficult to reach if backscatter transponders based on low-profile antennas such as patch antennas are used. The typical single-layer patch printed on a dielectric substrate is a narrow-band element. This well-known fact is mainly due to the limitations imposed by the dielectric substrate. For instance, to achieve the bandwidth, thicker substrates must be employed or enhancement bandwidth techniques must be considered [30]-[32]. Another challenge is the transponder detection. This can be improved increasing the differential radar cross section (RCS). To this end, an array of antennas can be used. However, increasing the number of FSS elements, the differential radar cross section can be easily increased as will be shown in this work. The cost that must be paid is an increase of the power consumption due to the large number of diodes during the forward state. However, reasonable values of RCS can be achieved with a small number of dipoles, for example with 10 dipoles with a current consumption of 2 mA assisted by a 3 V battery.

The paper is organized as follows. Section 2 deals about the basic theory of the backscattered transponder, using the active-controlled FSS. Section 3 describes a transponder designed as proof of concept. The design of the active reflecting surface is based on electromagnetic simulations. This section includes the experimental results yielded. Section 4 draws the conclusions.

2. Tag Based on Frequency Selective Surface

2.1 Range Measurement using Modulated Transponder

A block diagram of the proposed system is shown in Fig. 1. It is composed by the tag and the reader. In this case, a FMCW radar is used as a reader enabling the measurement of the tag to reader distance. The radar interrogates the tag which answers modulating its RCS. Depending on the application, data from sensors or identification codes can be sent back to the reader. The tag consists of a FSS loaded with PIN diodes that modulate the backscattered field of the tag (see Fig. 2).

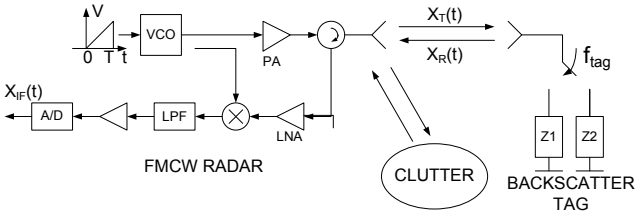

Fig. 1. Schematic block diagram of a FMCW radar using a modulated backscatter tag.

The determination of range of modulated backscatter transponders has been proposed in several works, see for example [8], [14], [17]. In this section, the basic theory of operation is summarized for completeness. The transmitted frequency is modulated by a saw teeth pulse of duration T. The transmitted signal is given by:

$$x_T(t) = A\cos\left(2\pi(f_c t + \frac{1}{2}\mu t^2)\right) \tag{1}$$

where A is the amplitude, f_c is the carrier frequency, $\mu = B/T$, T and B are the sweep slope, duration and bandwidth respectively.

The received signal is the transmitted signal attenuated, delayed by the time of flight between the transmitter and the tag, and modulated by the tag, with tag frequency f_{tag}:

$$x_R(t) = A'\cos\left(2\pi(f_c(t-\tau)+\frac{1}{2}\mu(t-\tau)^2\right)\cos\left(2\pi f_{tag}t+\phi_0\right) \quad (2)$$

where ($\tau = 2d/c$), d is the transmitter to tag distance and c is the speed of light, A' is the received amplitude, ϕ_0 is the phase associated to tag oscillator.

The IF-signal at the output of the mixer and low-pass filtered can be expressed as:

$$\begin{aligned} x_{IF}(t) &= A''\cos(2\pi(f_{tag}+\mu\tau)t+\phi_1) \\ &+A''\cos(2\pi(f_{tag}-\mu\tau)t+\phi_2) \end{aligned} \quad (3)$$

where A'' is the amplitude at the IF-output, and ϕ_1, ϕ_2, are phase constants generated from the mixing process that do not influence in the result.

To determine the mixing frequency, the time signal of the IF-signal is sampled. Then, a Fourier Transform and a peak search are carried out to obtain a raw frequency estimation. In practice, Fast Fourier Transform (FFT) with zero-padding or chirp Z transform can be used to improve the frequency resolution. In order to reduce side lobules effect due to time-windowing, the Hamming Window can be used instead of a Rectangular Window.

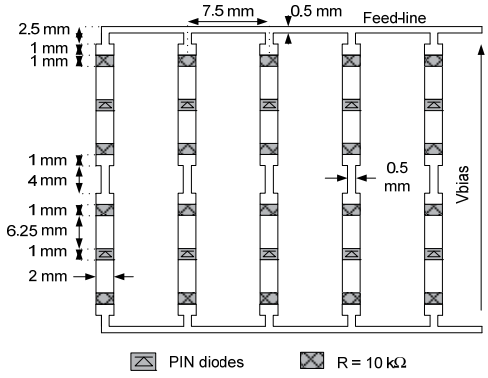

(a)

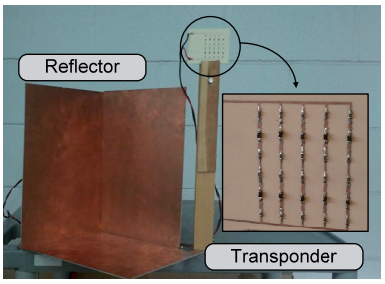

(b)

Fig. 2. (a) Diagram of a designed FSS (dimensions are included). (b) Transponder and reflector used in the measurement setup as reference.

From (3), the distance can be determined from the frequency offset between the couple of peaks in the spectrum around f_{tag}.

$$\Delta f = \mu\tau = \mu\frac{2d}{c} \rightarrow d = \frac{c}{2\mu}\Delta f \quad (4)$$

where Δf is the mixed frequency.

For a non-modulated target, $f_{tag}= 0$, the distance to the target is obtained using the well known FMCW radar equation:

$$d = \frac{c}{2}\mu\cdot\Delta f = \frac{cT}{2B}\cdot\Delta f \quad (5)$$

Assuming that the target is scanned during the entire sweep, the signal is windowed by a rectangular time-window of duration T. Therefore, the precision in the determination of the mixed frequency is about $1/T$. The range measurement resolution of the system can be mainly estimated as follows:

$$\Delta d = \frac{c}{2B}. \quad (6)$$

Hence it is proved that the range measurement resolution depends only on the sweep bandwidth.

The two cases (non-modulated tag and modulated target) are schematically shown in Fig. 3. In Fig. 3a the tag is difficult to be distinguished due to the phase noise and it is interfered by the strong clutter reflections. Whereas when the tag is modulated (Fig. 3b) a pair of peaks appears around f_{tag} whose separation is proportional to the distance (4). In this last case, the tag can be easily detected. Furthermore as the phase noise power decreases proportionally with the frequency, the noise floor is limited by the receiver noise figure. In consequence the signal to noise ratio is increased. To avoid aliasing, the maximum distance is limited by the modulated tag frequency and the sampling frequency:

$$f_{tag} - \mu\tau > 0, \quad (7)$$

$$f_{tag} + \mu\tau < f_s/2 \ . \quad (8)$$

Thus, the maximum non ambiguous distance is given by

$$d < \max\left\{\frac{cf_{tag}}{2\mu}, c\frac{f_s/2 - f_{tag}}{2\mu}\right\}. \quad (9)$$

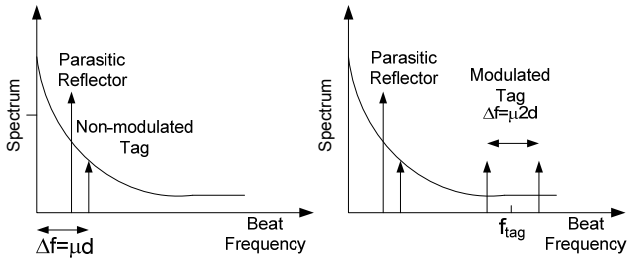

(a) (b)

Fig. 3. Spectrum after low-pass filter in the IF stage: (a) Non-modulated tag. (b) Modulated tag.

2.2 FSS as a Backscatter Modulator

When the transmitted signal hits the tag, a portion of the power is backscattered towards the receiver. The tag modulates the incident field by switching the PIN diodes that load the FSS. In this work, the FSS is made as in [28] by an array of dipoles. Fig. 2a shows a manufactured prototype of 10 dipoles and a photography is shown in Fig. 2b. Then, an active FSS can be viewed as an array of antennas loaded with the impedance of the PIN diodes. Hence, the backscattered field can be studied using fundamental antenna scattering theory [33], [34].

The backscattered field of an antenna can be split as a sum of two terms: a structural mode and an antenna mode, or a load-independent term and a load-dependent term, respectively:

$$\overline{E}_s(Z_L) = \overline{E}_{est} + \overline{E}_m \Gamma, \tag{10}$$

where $E_S(Z_L)$ is the scattered field by the tag connected to the load Z_L, E_{est} is the scattered field when the tag is connected to a reference load $Z_L = Z_a^*$, where Z_a is the antenna's impedance. Γ is the power reflection coefficient given by [33]: $\Gamma = (Z_L - Z_a^*)/(Z_L + Z_a)$.

When the load is the conjugate impedance of the antenna impedance, all the incident power is transferred to the load and the antenna only reflects the structural mode. The structural mode arises from the induced current on the antenna conducting surface by the incident wave, and it does not depend on the load. The structural mode depends on characteristics such as the antenna type, geometry, and material. Thus, the structural mode is independent of the load reflection coefficient, whereas the antenna mode is proportional to it.

By switching the PIN diodes that load the dipoles of the FSS, the reflect coefficient is modulated. As a first approximation the reflection coefficient can be approximated by a square waveform with amplitude $\Delta\Gamma$. It can be developed in a Fourier series:

$$\Gamma(f) = \sum_{n=-\infty}^{+\infty} c_n \delta(f - (f_c + n f_{tag})) \tag{11}$$

where c_n are the Fourier coefficients, and f_c is the input frequency of the incident signal that illuminates the tag. For a square waveform with duty cycle δ, the coefficients c_n are given by:

$$c_n = \begin{cases} \Gamma_{avg} & , n = 0 \\ \Delta\Gamma\,\delta\left(\dfrac{\sin n\pi\delta}{n\pi\delta}\right) & , n \neq 0 \end{cases} \tag{12}$$

where Γ_{avg} is the average power reflection coefficient between on and off states.

The backscattered field can be expressed as:

$$\begin{aligned} \overline{E}_s &= \left(\overline{E}_{est} + \overline{E}_m \Gamma_{avg}\right)\delta(f - f_c) \\ &+ \overline{E}_m \sum_{n\neq 0} c_n \delta(f - (f_c + n f_{tag})) \end{aligned} \tag{13}$$

Therefore, the first term in (13) results in the non-modulated term, and it depends on the structural mode of the tag. The second term represents the modulated sidebands that are function of the antenna mode. Considering the coefficients of higher amplitude in the Fourier expansion ($n = \pm 1$), results in the components at the frequencies $f_c \pm f_{tag}$. Therefore the received signal at the radar can be expressed by (2) after taking into account the propagation delays. The radar cross-section of a target is a far-field quantity that can be expressed as:

$$RCS = \lim_{d\to\infty} 4\pi d^2 \frac{\left|\overline{E}_s\right|^2}{\left|\overline{E}_i\right|^2}. \tag{14}$$

The differential RCS [29] is the RCS due to antenna mode that depends on the load reflection coefficient difference $\Delta\Gamma$ between the two modulated states (diodes on and off). The differential RCS can be expressed as [29]:

$$RCS_{dif} = \lim_{x\to\infty} 4\pi d^2 \frac{\left|\overline{E}_m c_1\right|^2}{\left|\overline{E}_{in}\right|^2} = \frac{\lambda^2}{4\pi} G^2 \left|\Delta\Gamma\right|^2 m \tag{15}$$

where λ is the wavelength, G is the tag gain, and m is a modulating factor that can be obtained from (12) as $m = |c_1|^2/|\Delta\Gamma|^2$.

In contrast with narrow-band RFID systems, here the differential RCS must be maximized in the entire radar frequency band.

3. Measurements and Results

3.1 FSS Design

Some prototypes of FSS have been manufactured following the guide lines described in [28]. The FSS are designed using Rogers 4003 substrate (relative permittivity $\varepsilon_r = 3.54$, loss tangent $\tan\delta = 0.003$, and height of 32 mil). The FSS are designed to cover the frequency band between 9.25 GHz and 10.75 GHz, which is the frequency band of the radar used in the experimental results (Siversima model RS3400X). Low-cost NXP BAP51-03 PIN diodes [35] are selected to reconfigure the response of the FSS.

In order to understand the operation of a tunable FSS, Fig. 4 shows schematically the reflectivity for the two ideal diode states: ON, where the diode is forward-biased, and OFF, where all the diodes are reverse-biased. It is known [20] that the FSS presents a high reflectivity when the frequency of the incident wave is close to the dipoles resonant frequency (when the dipoles become approximately half a wavelength). Therefore, the FSS can be modeled with a LC series equivalent circuit (Fig. 4) whose resonant frequency depends on the diode state. When the diodes are in state ON, their impedance theoretically should be a short circuit for an ideal diode, hence the FSS has a high reflectivity and RCS around the resonant frequency of the di-

poles. When the diodes are in state OFF, their impedance should theoretically be an open circuit. Under this load condition, the FSS is like an array of dipoles which are half long than the forward-biased case. As a consequence, the resonant frequency of the FSS loaded with an open circuit is about the double that the case in which the dipoles of the FSS are loaded with a short circuit. Therefore in this situation, the differential RCS should be higher between the two resonant frequencies.

The next rules are followed to design the FSS:

1) The dipole width chosen is much lower than the wavelength at the center frequency. In this case a 2 mm width is selected allowing a smooth diodes weld.

2) Once the width of the dipole arms is chosen, the length of the dipoles is computed to resonate at the low frequency edge of the radar band. Thus, the frequency band with high differential RCS covers the entire radar frequency band. A first approximation, assuming that the ideal diode in ON state is a short circuit, occurs when the length is a half-wavelength. As the FSS grid is printed on a dielectric then the resonance frequency becomes lower, especially for thick substrates. The effective permittivity can be estimated using results given in [20] (Appendix E). However, due to the end open capacitance effect, the resonance frequency is lower (about 10% depending on the dipole width). Due to the effect of diode parasitics, the resonance frequency of the FSS when the diodes are OFF is lower than in the ideal open circuit [28]. Therefore, the frequency band is reduced compared to an ideal diode case. These parasitic effects change the current distribution along the dipoles [20]. The influence of some of the above factors can be quantified theoretically leading to generic rules. The influence of the rest of the factors must be determined numerically or experimentally. Therefore electromagnetic simulations must be performed to study the bandwidth reduction and for the calculation of the dipoles length. Several simulation electromagnetic methods such as [20] can be employed to simulate. In this work, to perform the electromagnetic simulations a Finite Element Method in frequency domain implemented in the electromagnetic full-wave Ansoft HFSS software is used. The diode is taken into account in the simulator using a simplified lumped RLC equivalent circuit [28]. Fig. 4 shows the electrical circuit model of the BAP51-03 PIN diode [35] used in the simulation for the two-states. In the forward-biased case, the diode mainly represents a small resistance, which has small effect on the desired response of the FSS. Because of its small value, the series self inductance of the diode in this case should be considered for simulations. However, when it is reverse biased, the parasitic capacitance considerably deviates the position of the surface stop-band by altering the total effective capacitance of the unit cell. Therefore, it is necessary to consider its effect in the design process.

3) Small spacing between the dipoles generates a strong coupling between them and a reduction of the effective permittivity and consequently of the resonance frequency is produced. Moreover the effective area and the RCS are smaller. However, the spacing cannot be arbitrarily increased because it must be less than about 0.4 λ to avoid grating lobes [20]. Here, it is fixed to about a quarter-wavelength at the center frequency.

4) Metallic frames surrounding the FSS window may influence on its behavior. Therefore, the bias lines must be carefully designed. 10KΩ bias resistors are used to set the bias current to the diodes and they present high impedance that allows to isolate the bias lines and the dipoles. The bias lines between diodes are designed to be shorter than the length of the arms of the dipoles in order to resonate at a higher frequency, outside the frequency band of the radar. The other lines are orthogonal and isolated by the resistors. It has been checked that the bias lines have a small effect on the RCS within the radar frequency band.

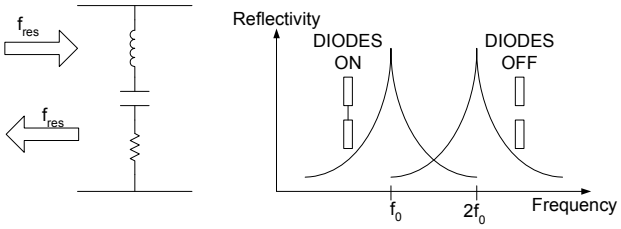

Fig. 4. Equivalent circuit model of the FSS. Reflectivity for the two diode states: State ON (diode is shorted). The waves whose frequencies are close to the resonance frequency are reflected. State OFF (diode is open-circuit), the FSS is transparent for these.

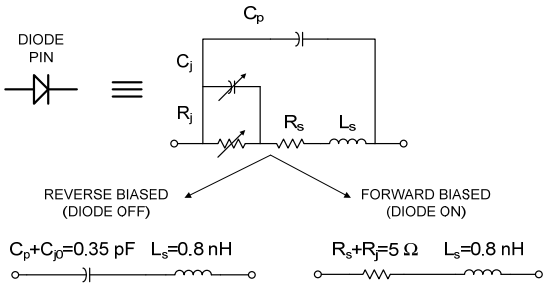

Fig. 5. High-frequency equivalent circuit for the PIN diode used.

Fig. 6 shows the simulation of the complex RCS (magnitude and angle) for the two diode states. FSS with the same spacing and dipole lengths but with different number of dipoles (3, 4 and 5), and the case of an FSS with 10 dipoles in two columns is considered. The length of the arm of the dipoles is 6.25 mm, the width of the dipoles is 2 mm, and the horizontal and vertical spacing are 7.5 mm and 9.25 mm, respectively (see Fig. 2a, a schema of a 10 dipoles prototype). Fig. 7 shows the differential RCS obtained subtracting the complex RCS for the two states. This figure shows that the level of the differential RCS increases because the effective area of the FSS increases, but also that the bandwidth increases with the number of dipoles. A peak of differential RCS is obtained when the phase differences between the two diode states are maximum,

which happens approximately at the middle frequency between the two resonances (when diodes are ON and OFF). For practical applications, the number of the FSS dipoles may be limited by its power consumption. In this case, it is limited to 2 mA, considering an FSS made with 10 dipoles. From (13), the differential RCS of a backscattering antenna can be computed. Using a 10-dipole FSS, the differential RCS is the same as modulating an antenna with a gain of 13.5 dB at 10 GHz, assuming the same modulating factor *m*. To achieve this gain using a low-profile antenna, an array of wideband patches should be used.

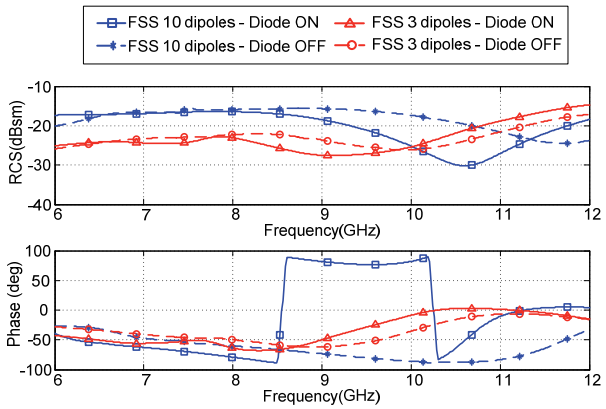

Fig. 6. Complex RCS (magnitude, top figure) and phase (bottom figure) in two different tags when the diode is shorted or open-circuit.

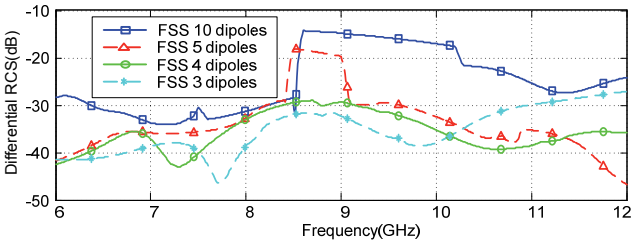

Fig. 7. Differential RCS of different tags as function of the number of dipoles.

3.2 Experimental Results

In order to characterize the frequency behavior of the differential RCS, the experimental setup described in Fig. 8 has been used. A 20 dB standard horn antenna is connected to a signal generator (Rhode SMF-100) and it was used to illuminate the tag with a CW. The FSS is biased with a low-frequency sinusoidal generator that generates a 50 kHz 3Vpp sinusoidal signal (Agilent 33521A). This signal is used to switch the diodes of the FSS. A receiver horn antenna is connected to the spectrum analyzer (Rohde FSP-30). Microwave absorbers are used to reduce multipath interference. Fig. 9.a shows an example of the spectrum measured by the spectrum analyzer when a 3-dipole FSS is illuminated at 10 GHz. A strong peak at the transmitted frequency due to the coupling between transmitter and receiver antenna can be observed. The sideband peaks are originated by the modulation of the tag and the frequency space between each other is the modulation frequency (50 kHz). Due to the clipping effect of the diodes, the spectrum is very similar to that of a square signal (sinc function). Therefore, the amplitude of the sideband is proportional to the differential RCS (15). Fig. 9.b compares the received power of different RCS after a correction of the antennas' gain is done. This figure shows that the received power and the bandwidth increase with the number of dipoles. The measurements show a frequency dependence of the differential RCS, in agreement with simulations of Fig. 7. The small difference is probably due to parasitic effects that have not been taken into account in the diode model during the simulations. For instance, it can be observed that the frequency response has a flatness of 2 dB for the case of a FSS with 10 dipoles.

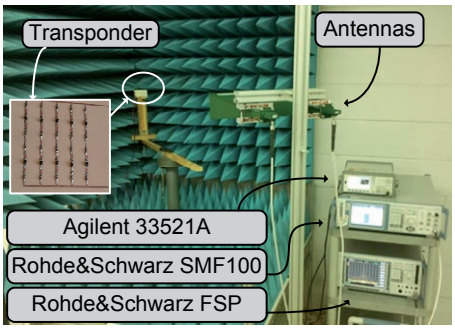

Fig. 8. Photography of the system used for modulation characterization.

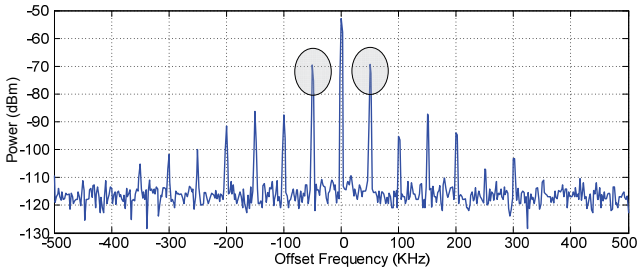

(a)

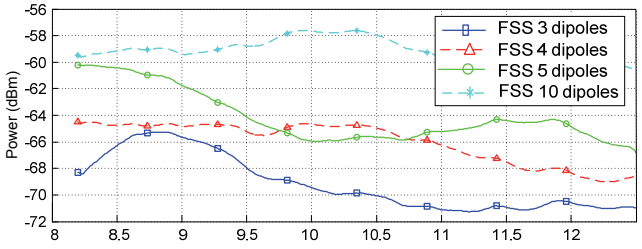

(b)

Fig. 9. a) Measurement of the spectrum at 10 GHz. b) Comparison of the received power for different RCS after the gain of the antennas was corrected.

Commercial radar from Siversima, Sweden (model RS3400X/00) is used to demonstrate the viability of the proposed solution. The RS3400X/00 is a synthesizer, X-band, FMCW radar front end. The nominal transmitted power of the radar module is 0 dBm+/-5 dB. The radar sweeps the 9.25-10.75 GHz frequency band with a sweep

time of 75 ms and it is connected to a 20 dB standard pyramidal horn. The IF signal is sampled at 20 kHz. Then the chirp Z transform (a variant of FFT that does not require zero padding to increase the frequency resolution) is applied to compute the IF spectrum. A Hamming Window is applied before computing the spectrum. A 90º rectangular dihedral reflector (20 cm by 29 cm) is located close to the tag (see Fig. 2b). This reflector presents a high RCS (19.7 dB oriented to the radar) and it is used as a reference for comparison purposes. Therefore, the reflector introduces a strong interference to the backscattered signal from the tag. The FSS is modulated at 5 kHz. Fig. 10 shows some results at different distances (at 2 m and 10 m). Photography of the experimental setup is shown in Fig. 11. Without modulation, the tag signal cannot be detected because it is masked by the strong reflection of the reflector, clutter and phase noise interference. However, when the tag is modulated, two peaks appear at the spectrum of the IF signal around the frequency modulation. Furthermore, some clutter removal can be achieved if the non-modulated signal is subtracted. When the distance increases, the separation of the frequency sidebands increases according to the theory presented. The received power and the signal to noise ratio decrease if the distance increases as it can be viewed in the case of 10 m. Fig. 12 shows the estimated distance obtained from the measurement considering the presence of the reflector that is also employed as a reference and derived from the spacing between the sideband peaks. A systematic offset between the measured and the real distance from the radar to the transponder is due to the delay produced by the length of cables, which connect the radar and the antenna. This systematic offset has been subtracted. Good agreement is obtained between the two measurements. It can be noticed that the standard deviation error between the measurements of the reflector distance (17 cm) and the tag distance (11 cm) fall within the radar resolution given by (6) (in this case, 10 cm).

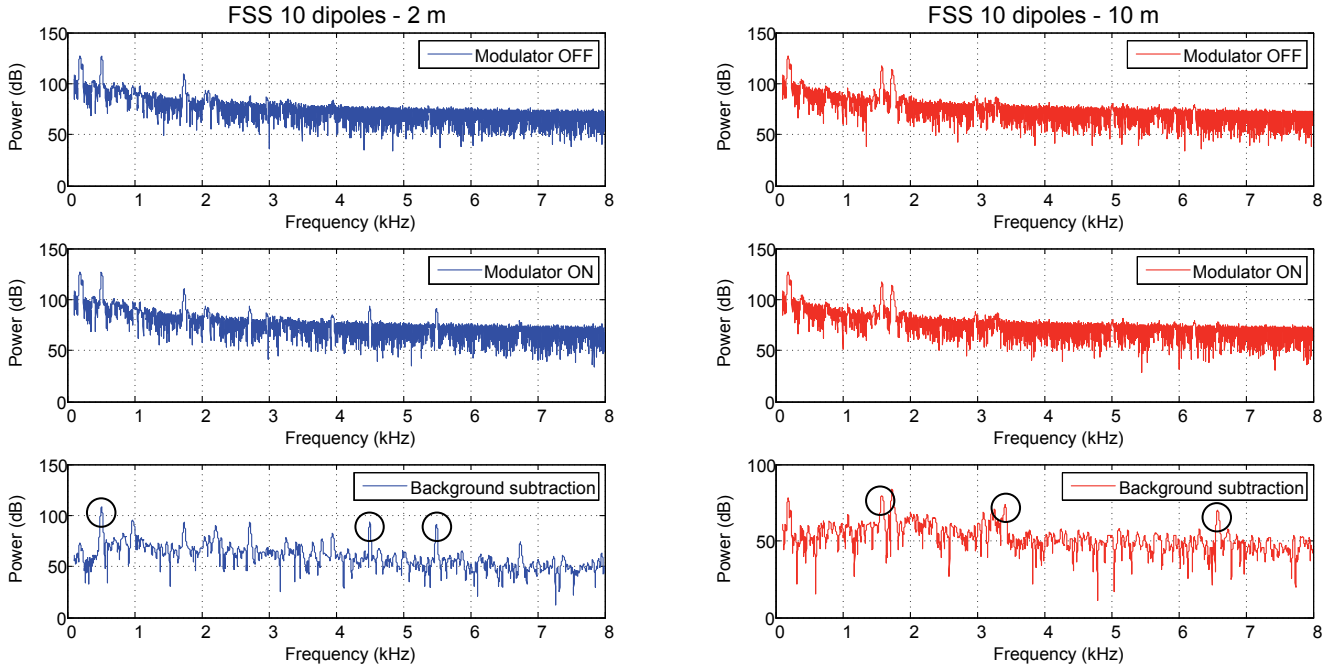

Fig. 10. Measurement comparison of the tag and the reflector at 2 m and 10 m. Tag measurements in case of no modulation, or with f_{tag} = 5 kHz modulation. The background subtraction technique permits to recover the peaks clearly (black circles).

Ref.	*Technology*	*Central Frequency (GHz)*	*Bandwidth (MHz)*	*Radar EIRP (dBm)*	*Measured Range*	*Comments*
18	Synchronized VCO	5.8	150	10	550 m outdoor	Very large power consumption and complexity
19	Switched Injection-Locked Oscillator	5.8	140	14	25 m indoor 200 m outdoor	Large Power Consumption (60 mW)
16	Modulated Backscatter antenna	76	1000	20	3.8 m anechoic chamber	22 mA/5 V (110 mW) GaAs PIN MMIC switch
17	Switched Van Atta array	5.8	100	14	20 m indoor	Moderate power consumption 8 PIN SPSTs. Complex antenna array design
This work	Active modulated FSS	10	1500	15	12 m indoor	2 mA/3 V (6 mW), Low Cost PIN diodes. Easy and scalable design

Tab. 1. Comparison with existing transponder technologies.

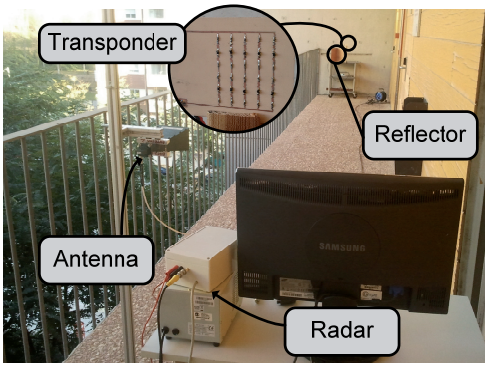

Fig. 11. Photography of the measurement system.

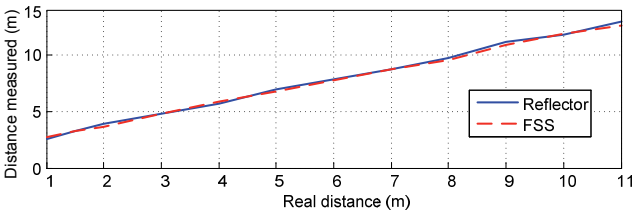

Fig. 12. Estimated distance obtained from the reflector measurements (solid line) and distances derived from the spacing between the sideband peaks (dashed line).

In Tab. 1 a comparison between the results obtained above and the ones obtained applying other technologies based on FMCW radar are made. The first two rows describe two technologies based on different secondary radar solutions [18], [19]. The third row is based on a modulated backscatter transponder [16]. The main characteristic of Van Atta architecture [17] is described in the fourth row. Finally, the last row shows the results reached in this work. It can be seen that the power consumption of the active secondary radar solutions is notably higher than the other technologies and it is also a more complex solution. On the other hand, the range in secondary radar systems is higher because the signal is regenerated. Therefore the attenuation ideally decreases with the square of distance in free-space channel, whereas in the other transponders the received power is inversely proportional to the distance raised to the fourth. In the case of modulated solutions (the last three cases), the range depends on the frequency, the transmitted power and receiver sensitivity. When the frequency increases, the free-space path loss increases and thus the range is reduced. The results of this work evidence that a moderate range and high resolution (high bandwidth) can be achieved with a low power consumption and a low cost. Although several diodes are used, it does not need to flow large currents, because the impact in the differential RCS of the FSS is small. The main impact in the differential RCS is due to the OFF state of the diodes that is determined by the parasitic elements, but in this situation the current is nearly zero and does not affect to the power consumption. In Van Atta architectures, the power consumption of the PIN switch is generally high in order to reduce the insertion losses. On the other hand when the frequency of operation increases, the cost and power consumption of the switching elements also increases. The proposed FSS is easily frequency scalable adjusting the length and the spacing of the dipoles, if the design rules given above are followed. The designs at millimeter frequencies require diodes with low capacitance and parasitic inductances, thus the cost and mounting complexity increases if flip-chip diodes or chip MMIC soldered with wire bonding are required.

4. Conclusions

This work has studied the feasibility to use actively controlled frequency selective surfaces (FSS) with FMCW radars. The communication between the tag and the reader is produced using the backscattering technique. The basic operation theory of the system is explained. In order to increase the tag detection the maximization of the differential RCS is required. These types of radars are used in applications in which a good range resolution proportional to the bandwidth must be guaranteed. Hence, the FSS must support this bandwidth. The simulations and experimental results show that the bandwidth of a standard FMCW radar is enough to exploit FSS in these conditions. Given that the RCS is modulated, interference from non-modulated clutter can be removed using a simple background subtraction technique that consists on subtracting the modulated and not modulated tag measurements. This technique is essential to be applied in indoor scenarios or in applications in which strong clutter from reflectors are presented. An experimental setup based on commercial low-power FMCW radar working as a reader is proposed to measure the modulated radar cross section of the tags. Good results are obtained up to 11 m using the Fig. 1 configuration in spite of the presence of a reflector.

Acknowledgements

This paper was supported by Spanish Government Project TEC2011-28357-C02-01 and BES-2012-053980.

References

[1] SKOLNIK, M. I. *Introduction to Radar Systems*. 2nd ed. Singapore: McGraw-Hill, 1981.

[2] BRUMBI, D. Low power FMCW radar system for level gauging. In *IEEE MTT-S International Microwave Symposium Digest*. Boston, MA (USA), 2000, vol. 3, p. 1559–1562.

[3] ROHLING, H., MEINECKE, M.-M. Waveform design principles for automotive radar systems. In *Proceedings CIE International Conference on Radar*. Beijing (China), 2001, p. 1–4.

[4] JEONG, S.-H., YU, H.-Y., LEE, J.-E., OH, J.-N., LEE, K.-H. A multi-beam and multi-range radar with FMCW and digital beam forming for automotive applications. *Progress in Electromagnetics Research*, 2012, PIER 124, p. 285–299.

[5] HUANG, Y., BRENNAN, P. V., PATRICK, D., WELLER, I., ROBERTS, P., HUGHES, K. FMCW based MIMO imaging radar

for maritime navigation. *Progress in Electromagnetics Research*, 2011, vol. 115, p. 327–342.

[6] RALSTON, T. S., CHARVAT, G. L., PEABODY, J. E. Real-time through-wall imaging using an ultrawideband multiple-input multiple-output (MIMO) phased array radar system. In *IEEE International Symposium on Phased Array Systems and Technology (ARRAY)*. Waltham (MA, USA), 2010, p. 551–558.

[7] ANITORI, L., DE JONG, A., NENNIE, F. FMCW radar for life-sign detection. In *IEEE Radar Conference*. Pasadena (CA, USA), 2009, p. 1–6.

[8] VOSSIEK, M., ROSKOSCH, R., HEIDE, P. Precise 3-D object position tracking using FMCW radar. In *29th European Microwave Conference*. Munich (Germany), 1999, vol. 1, p. 234–237.

[9] HUANG, Y., BRENNAN, P. V., SEEDS, A. Active RFID location system based on time-difference measurement using a linear FM chirp tag signal. In *IEEE 19th International Symposium on Personal, Indoor and Mobile Radio Communications (PIMRC)*. Cannes (France), 2008, p. 15–18.

[10] BRUGGER, M., CHRIST, T., KEMETH, F., NAGY, S., SCHAEFER, M., PIETRZYK, M. M. The FMCW technology-based indoor localization system. In *Ubiquitous Positioning Indoor Navigation and Location Based Service (UPINLBS)*. Kirkkonummi (Findland), 2010, p. 1–6.

[11] THAI, T. T., CHEBILA, F., MEHDI, J. M., PONS, P., AUBERT, H., DEJEAN, G. R., TENTZERIS, M. M., PLANA, R. Design and development of a millimetre-wave novel passive ultrasensitive temperature transducer for remote sensing and identification. In *European Microwave Conf.* Paris (France), 2010, p. 45–48.

[12] AUBERT, H., CHEBILA, F., JATLAOUI, M., THAI, T., HALLIL, H., TRAILLE, A., BOUAZIZ, S., RIFAI, A., PONS, P., MENINI, P., TENTZERIS, M. Wireless sensing and identification of passive electromagnetic sensors based on millimetre-wave FMCW radar. In *IEEE International Conf. on RFID-Technologies and Applications (RFID-TA)*. Nice (France), 2012, p. 398–403.

[13] PONS, P., AUBERT, H., MENINI, P., TENTZERIS, M. Wireless passive autonomous sensors with electromagnetic transduction. In *International Conference on Microwave and High Frequency Heating*. Toulouse (France), 2011.

[14] THORNTON, J., EDWARDS, D. J. Range measurement using modulated retro-reflectors in FM radar system. *IEEE Microwave Guided Wave Lett.*, 2000, vol. 10, p. 380–382.

[15] KOSSEL, M., BENEDICKTER, H. R., PETER, R., ÄCHTOLD, W. Microwave backscatter modulation systems. *In IEEE Int. Microwave Symp. Dig.* Boston (MA, USA), 2000, p. 1427–1430.

[16] SCHMID, C. M., FEGER, R., STELZER, A. Millimeter-wave phase-modulated backscatter transponder for FMCW radar applications. In *IEEE MTT-S International Microwave Symposium Digest (MTT)*. Baltimore (MD, USA), 2011.

[17] MARCACCIOLI, L., SBARRA, E. URBANI, L., GATTI, R. V., SORRENTINO, R. An accurate indoor ranging system based on FMCW radar. In *IEEE Intelligent Vehicles Symposium (IV)*. Baden-Baden (Germany), 2011, p. 981–986.

[18] RÖHR, S., GULDEN, P., VOSSIEK, M. Precise distance and velocity measurement for real time locating using a frequency modulated continuous wave secondary radar approach. *IEEE Transactions on Microwave Theory and Techniques*, 2008, vol. 56, no. 10, p. 2329–2339.

[19] VOSSIEK, M., GULDEN, P. The switched injection-locked oscillator: A novel versatile concept for wireless transponder and localization systems. *IEEE Transactions on Microwave Theory and Techniques*, 2008, vol. 56, no. 4, p. 859–866.

[20] MUNK, B. A. *Frequency Selective Surfaces*. New York: Wiley, 2000.

[21] MUNK, B. A., KOUYOUMJIAN, R. G., PETERS, L. Reflection properties of periodic surfaces of loaded dipoles. *IEEE Trans. on Antennas and Prop.*, 1971, vol. AP-19, no. 5, p. 612–617.

[22] IZQUIERDO, B. S., PARKER, E. A., ROBERTSON, J. B., BATCHELOR, J. C. Tuning technique for active FSS arrays. *Electron.Letters*, 2009, vol. 45, p. 1107–1109.

[23] CHANG, T. K, LANGLEY, R. J., PARKER, E. A. Active frequency-selective surfaces. *IEE Proceedings - Microwaves, Antennas and Propagation*, 1996, vol. 143, no. 1, p. 62–66.

[24] CHE, Y., HOU, X., GAO, Z. A tunable miniaturized-element frequency selective surfaces without bias network. In *IEEE International Conference on Microwave Technology & Computational Electromagnetics (ICMTCE)*. Beijing (China), 2011, p. 70–73.

[25] KIANI, G. I., BIRD, T. S., FORD K. L. 60 GHz ASK modulator using switchable FSS. In *IEEE Antennas and Propagation Society International Symposium (APSURSI)*. Toronto (Canada), 2010, p. 1–4.

[26] KIANI, G. I., BIRD, T. S. Amplitude shift keying modulator based on switchable FSS for terahertz applications. *Journal of Radio Science*, 2011, vol. 46, RS2015.

[27] NEELAKANTA, P. S., STAMPALIA, A. K., DE GROFF, D. An actively-controlled microwave reflecting surface with binary-pattern modulation. *Microwave Journal*, 2003, vol. 46, no. 12, p. 22–35.

[28] LAZARO, A., RAMOS, A., GIRBAU, D. VILLARINO, R. A novel UWB RFID tag using active frequency selective surface. *IEEE Transactions on Antennas and Propagation*, 2013, vol. 61, no. 3, p. 1155–1165.

[29] NIKITIN, P. V., RAO, K. V. S., LAM, S. F., PILLAI, V., MARTINEZ, R., HEINRICH, H. Power reflection coefficient analysis for complex impedances in RFID tag design. *IEEE Trans. Microwave Theory Tech.*, 2005, vol. 53, no. 9, p. 2721–2725.

[30] TARGONSKI, S. D., WATERHOUSE, R. B., POZAR, D. M. Design of wide-band aperture-stacked patch microstrip antennas. *IEEE Transactions on Antennas and Propagation*, 1998, vol. 46, no. 9, p. 1245–1251.

[31] POZAR, D. M., KAUFMAN, B. Increasing the bandwidth of a microstrip antenna by proximity coupling. *Electronics Letters*, 1987, vol. 23, no. 8, p. 368–369.

[32] POZAR, D. M. Microstrip antennas. *Proceedings of the IEEE*, 1992, vol. 80, no. 1, p. 79–91.

[33] COLLIN, R. E., ZUCKER, F. J. *The Receiving Antenna. Antenna Theory 1*. New-York: McGraw-Hill, 1969.

[34] GREEN, R. B. *The General Theory of Antenna Scattering*. ElectroScience Laboratory, Columbus (OH, USA), 1963. Rep. 1223–17.

[35] BAP51-03. General purpose PIN diode (datasheet), NXP, 2004. [Online] Cited 2014-02-27. Available at http://www.nxp.com/documents/data_sheet/BAP51-02_N.pdf

About Authors ...

Antonio LAZARO was born in Lleida, Spain, in 1971. He received the M.S. and Ph.D. degrees in Telecommunication Engineering from the Universitat Politècnica de Catalunya (UPC), Barcelona, Spain, in 1994 and 1998, respectively. He then joined the faculty of UPC, where he currently teaches a course on microwave circuits and antennas. In

July 2004 he joined the Department of Electronic Engineering, Universitat Rovira i Virgili, Tarragona, Spain. His research interests are microwave device modeling, on-wafer noise measurements, monolithic microwave integrated circuits (MMICs), low phase noise oscillators, MEMS, and microwave systems.

Javier LORENZO was born in Reus, Spain, in 1978. He received the Telecommunications Technical Engineering degree and MS in Electronics Engineering from Universitat Rovira i Virgili, Tarragona, Spain, in 2009 and 2011 respectively. Since September 2011 he is a researcher in his PhD at Universitat Rovira i Virgili, Tarragona, Spain. His research activities are oriented to microwave devices and systems, with emphasis on UWB, RFIDs, wireless sensors, radiometry and positioning.

Ramon VILLARINO received the Telecommunications Technical Engineering degree from the Ramon Llull University (URL), Barcelona, Spain in 1994, the Senior Telecommunications Engineering degree from the Universitat Politècnica de Catalunya (UPC), Barcelona, Spain in 2000 and the PhD from the UPC in 2004. During 2005-2006, he was a Research Associate at the Technological Telecommunications Center of Catalonia (CTTC), Barcelona, Spain. He worked at the Universitat Autonòma de Catalunya (UAB) from 2006 to 2008 as a Researcher and Assistant Professor. Since January 2009 he is a Full-Time Professor at Universitat Rovira i Virgili (URV). His research activities are oriented to radiometry, microwave devices and systems, based on UWB, RFIDs and frequency selective structures using MetaMaterials (MM).

David GIRBAU received the BS in Telecommunication Engineering, MS in Electronics Engineering and PhD in Telecommunication from Universitat Politècnica de Catalunya (UPC), Barcelona, Spain, in 1998, 2002 and 2006, respectively. From February 2001 to September 2007 he was a Research Assistant with the UPC. From September 2005 to September 2007 he was a Part-Time Assistant Professor with the Universitat Autònoma de Barcelona (UAB). Since October 2007 he is a Full-Time Professor at Universitat Rovira i Virgili (URV). His research interests include microwave devices and systems, with emphasis on UWB, RFIDs, RF-MEMS and wireless sensors.